PERGAMON

International Journal of Solids and Structures 40 (2003) 6877–6896

INTERNATIONAL JOURNAL OF SOLIDS and STRUCTURES

www.elsevier.com/locate/ijsolstr

On higher gradients in continuum-atomistic modelling

R. Sunyk, P. Steinmann *

Chair for Applied Mechanics, Department of Mechanical Engineering, University of Kaiserslautern, P.O. Box 3049, 67653 Kaiserslautern, Germany

Received 16 July 2002

Abstract

Continuum-atomistic modelling denotes a mixed approach combining the usual framework of continuum mechanics with atomistic features like e.g. interaction or rather pair potentials. Thereby, the kinematics are typically characterized by the so-called Cauchy–Born rule representing atomic distance vectors in the spatial configuration as an affine mapping of the atomic distance vectors in the material configuration in terms of the local deformation gradient. The application of the Cauchy–Born rule requires sufficiently homogeneous deformations of the underlying crystal. The model is no more valid if the deformation becomes inhomogeneous. Nevertheless the development of microstructures with inhomogeneous deformation is inevitable. In the present work, the Cauchy–Born rule is thus extended to capture inhomogeneous deformations by the incorporation of the second-order deformation gradient. The higher-order equilibrium equation as well as the appropriate boundary conditions are presented for the case of finite deformations. The constitutive law for the Piola–Kirchhoff stress and the additional higher-order stress are represented for the simplified case of pair potential-based energy density functions. Finally, a deformation inhomogeneity measure is introduced and studied for a particular non-homogeneous simple-shear like deformation.

Keywords: Cauchy–Born rule; Continuum-atomistic bridging; Higher-order continua

1. Introduction

Multiscale simulation methods in computational material science have matured considerably during the last decade. Among a large number of various approaches the techniques using semi-empirical energy potential functions stemming directly from lattice statics or dynamics, see e.g. Phillips (2001), Shenoy et al. (1999), Arroyo and Belytschko (2002) and Nakane et al. (2000), could be highlighted. Thereby, the continuum quantities such as the stress tensor or the tangent operator can be represented in terms of the derivatives of these potentials and depend consequently on the atomistic forces and stiffnesses. Noteworthy, the quasi-continuum framework advocated by Tadmor (1996) and Tadmor et al. (1999) consists of two

* Corresponding author. Tel.: +49-631-205-2419; fax: +49-631-205-2128.
E-mail address: ps@rhrk.uni-kl.de (P. Steinmann).
URL: http://mechanik.mv.uni-kl.de/.

0020-7683/$ - see front matter © 2003 Elsevier Ltd. All rights reserved.
doi:10.1016/j.ijsolstr.2003.07.001

different approaches. Thereby in particular the local or, in our terminology continuum-atomistic approach is only valid as long as the deformation field remains sufficiently homogeneous. If the deformation becomes non-homogeneous the non-local, or in our terminology the atomistic-continuum approach is more appropriate. An essential ingredient of the former, i.e. the continuum-atomistic approach is the Cauchy–Born rule (CBR) stemming from Born and Huang (1954) which states essentially that all atoms of a single crystal volume follow the prescribed displacement of its boundary, see Milstein (1982), Ericksen (1984), Zanzotto (1996). The validity of the CBR is studied e.g. by Friesecke and Theil (2002), whereby it turns out that the CBR fails for sufficiently large deformations.

We aim in the continuous description during the whole simulation. Since the application of the standard Cauchy–Born rule leads to the loss of the infinitesimal rank-one convexity at critical deformation states as investigated in our recent works (Sunyk and Steinmann, 2001a,b) a relaxation procedure is required to insure the existence of a solution of the original energy minimization problem, see e.g. Tadmor et al. (1999) or Chipot and Kinderlehrer (1988). Nevertheless the relaxation results in the development of microstructures with deformation inhomogeneity at the atomic length scale, for a motivating example see Fig. 1. To stay within the realm of the continuum-atomistic model and nevertheless to still obtain accurate results in this more general case of inhomogeneous deformations we consider the CBR in the classical form as the first term of a Taylor's series expansion of the deformation field and enhance this expansion by the second quadratic term including the higher-order deformation gradient. Based on this advanced kinematics we build a full higher-order gradient framework by minimization of the total energy of the body of interest. For the case of the loss of rank-one convexity the introduction of higher-order gradients is moreover motivated from studies on localization limiters, see e.g. Fleck and Hutchinson (1996). This framework is similar to the Toupin–Mindlin theory of linear elasticity, see Toupin (1962) and (Mindlin, 1964, 1965). Recently, the higher-order gradient theory for finite deformation has been elaborated by Geers et al. (2001) and Kouznetsova et al. (2002) within classical continuum mechanics in the context of homogenization approaches. A comparison of the various higher-order gradients theories can be found in the detailed overview elaborated by Fleck and Hutchinson (1996).

The new aspects of this contribution are a compact tensor format for all derivations and results; an application of the continuum-atomistic principles within the second-order theory summarized in Eqs. (30)–(34); a study of the relevance of the second-order theory for a non-homogeneous deformations on the basis

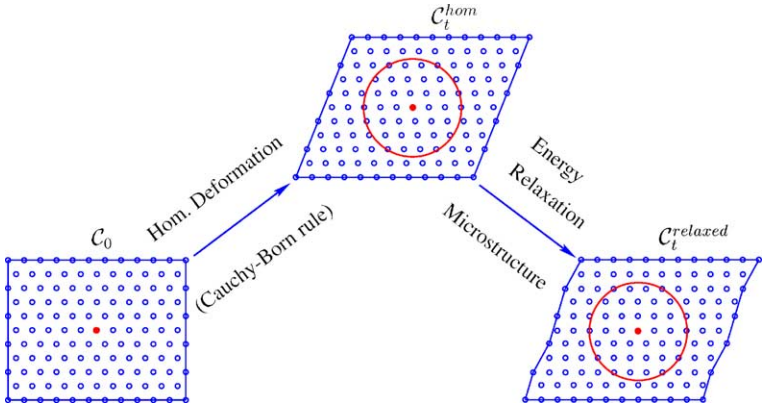

Fig. 1. Material configuration $\mathscr{C}_0$ and two spatial configurations: $\mathscr{C}_t^{\text{hom}}$ deformed homogeneously according to the Cauchy–Born rule and $\mathscr{C}_t^{\text{relaxed}}$ obtained during the energy minimization procedure by relaxation. Red circles display an interaction or cut-off-circle of the middle atom depicted in red and contain the current next neighbours of this atom. Atomic displacements within the cut-off-circle in $\mathscr{C}_t^{\text{relaxed}}$ are no more homogeneous and cannot be captured by the standard Cauchy–Born rule. (For interpretation of the references in colour in this figure legend, the reader is referred to the web version of this article.)

of a simple example; an introduction of the deformation inhomogeneity measure to characterize the change of the deformation field within the interaction circle.

The paper is organized as follows. The main definitions from quasi-static atomistic modelling are given in Section 2; Section 3 contains the detailed description of the continuum-atomistic modelling of the first as well as the second-order. In Section 4 a study of an example for a non-homogeneous deformation field is carried out and a deformation inhomogeneity measure is introduced. The conclusions in Section 5 close the paper.

2. Atomistic constitutive modelling

To set the stage and to introduce several definitions we start with a short review of the direct atomistic approach, whereby we restrict ourselves to classical lattice statics. For an overview on different approaches towards nanomechanics we refer to Ortiz and Phillips (1999). We consider a crystallite body consisting of N interacting atoms. The kinematics are then typically represented by the distance vectors between two atoms labeled i and j, i.e. $\boldsymbol{R}_{ij}$ and $\boldsymbol{r}_{ij}$ in the material and in the spatial configuration, respectively

$$\boldsymbol{R}_{ij} = \boldsymbol{R}_i - \boldsymbol{R}_j \quad \boldsymbol{r}_{ij} = \boldsymbol{r}_i - \boldsymbol{r}_j \quad \text{with} \quad r_{ij} = |\boldsymbol{r}_{ij}| \tag{1}$$

The position vectors $\boldsymbol{R}_i$ and $\boldsymbol{r}_i$ in both configurations are connected by the non-linear discrete map $\boldsymbol{\varphi}_i(\boldsymbol{R}_i)$, see Fig. 2. There are many well-known empirical energy functions describing the inter-atom interaction. In their simplest form these empirical potentials contain only pair-wise interactions Φ. Well-known examples for this type of pair potentials are e.g. Morse, Buckingham and Lennard-Jones potentials, which are functions of only the relative scalar distances $r = |\boldsymbol{r}|$ between two atoms. For instance, the celebrated Lennard-Jones potential used as a prototype model in the present work (see Fig. 3) has the format

$$\Phi(r) = 4\varepsilon\left[\left[\frac{\sigma}{r}\right]^{12} - \left[\frac{\sigma}{r}\right]^{6}\right] \tag{2}$$

with ε and σ denoting parameters to be fitted. In summary, the energy contribution of the atom i can be represented as a sum over pair-wise interactions of this atom with all other atoms in the body

$$E_i = \frac{1}{2}\sum_{j\neq i}\Phi(r_{ij}) \equiv \frac{1}{2}\sum_{j\neq i}\Phi_{ij} \tag{3}$$

Clearly, more sophisticated models are conceivable and indeed often necessary. For example many important properties of real solids are determined by their electronic structure. Therefore, it is very significant to include the dependence of the interaction energy on quantum mechanical effects. This problem has been treated e.g. in the work of Baskes and Daw (1983), who developed the so called Embedded Atom Method (EAM). Here each atom in a solid is viewed as an impurity embedded in the host consisting of all other

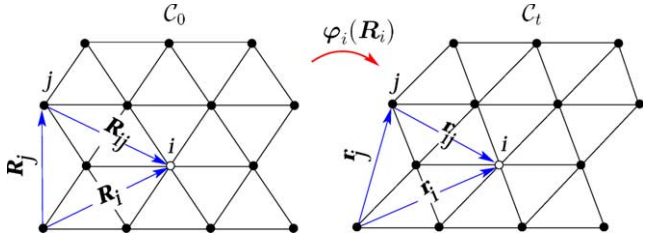

Fig. 2. Material $\mathscr{C}_0$ and spatial $\mathscr{C}_t$ crystal lattice configuration.

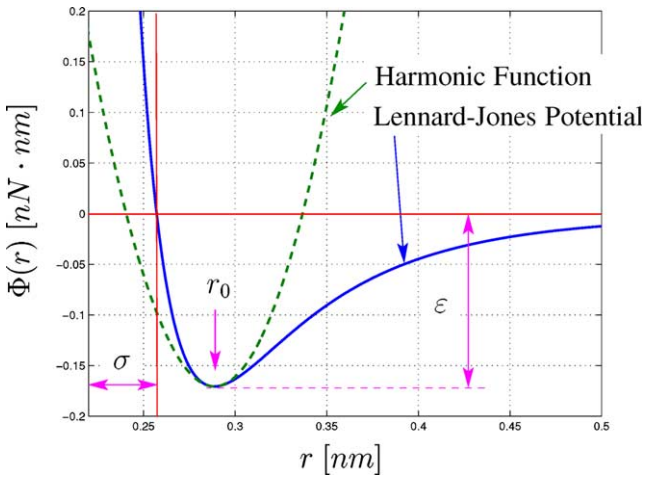

Fig. 3. The Lennard-Jones potential with parameters $\sigma = 0.257$ and $\varepsilon = 0.171$ (solid line) compared with the harmonic potential function (dashed line).

atoms. Thereby the energy E_i of the ith atom consists of two different terms: (1) the embedding energy $\overline{E}_i(\rho_i)$ of atom i, see Puska et al. (1981), i.e. the energy of the atom in a uniform electron gas relative to the atom separated from the electron gas, and (2) the contributions Φ_{ij} of the inter-ion interactions. It can be represented as follows

$$E_i = \overline{E}_i(\rho_i) + \frac{1}{2}\sum_{j\neq i} \Phi_{ij} \quad \text{with} \quad \rho_i = \sum_{j\neq i} \bar{\rho}_j(r_{ij}) \tag{4}$$

The embedding energy depends on the host electron density ρ_i at the position $\boldsymbol{r}_i$ before the atom i has been embedded and is an implicit function of the relative distances r_{ij}. Necessarily E_i is a function of these distances, too. Nevertheless, for the purpose of transparency we restrict ourselves in this work to only pairwise inter-atom interactions, thus all subsequent formulae are given under this limitation. In particular, without loss of generality, we will use the simple Lennard-Jones potential for the sake of demonstration. Finally, the total internal energy E^{int} of the crystal lattice can be represented as a sum over all atomic contributions

$$E^{\text{int}} = \sum_i E_i \tag{5}$$

Then the derivative of the total internal energy E^{int} with respect to the position vector $\boldsymbol{r}_i$ of the ith atom yields the force $\boldsymbol{f}_i$ acting on this particular atom due to the interactions with all other atoms

$$\boldsymbol{f}_i = -E^{\text{int}}_{,\boldsymbol{r}_i} = \sum_{j\neq i} \boldsymbol{f}_{ij} \quad \text{with} \quad \boldsymbol{f}_{ij} = -\frac{\Phi'_{ij}}{r_{ij}}\boldsymbol{r}_{ij} \tag{6}$$

whereby the comma denotes partial differentiation and the prime $(\bullet)'$ denotes the derivative of $(\bullet)$ with respect to r_{ij}, see e.g. Allen and Tildesley (1987), Eq. (5.2). Consequently $\boldsymbol{f}_{ij}$ represents the force acting on the atom i due to the atom j, see Fig. 4. This relation represents the underlying constitutive law of classical lattice statics based on only pair-potential interactions. Please note that here the summation convention is not adopted to quantities related to atomistics. The principle of the minimum of the total potential energy representing the global equilibrium results locally in the equilibrium at each atom

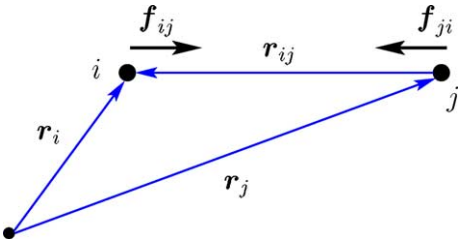

Fig. 4. Definitions of the distance vectors r_{ij} and the interaction force f_{ij}.

$$E^{\text{tot}} = E^{\text{int}} + E^{\text{ext}} \rightarrow \min_{r_i} \iff \sum_{j \neq i} f_{ij} + f_i^{\text{ext}} \doteq \mathbf{0} \tag{7}$$

with the external force f_i^{ext} acting on the atom i. Within an iterative solution strategy, the second derivative of the total energy E^{tot} with respect to r_j is needed. This results in the atomic level stiffness k_{ij}, whereby we obtain the particular result

$$k_{ij} = -E^{\text{int}}_{,r_i r_j} = \frac{\Phi'_{ij}}{r_{ij}} I + \left[\frac{\Phi''_{ij}}{r_{ij}^2} - \frac{\Phi'_{ij}}{r_{ij}^3} \right] r_{ij} \otimes r_{ij}, \quad i \neq j \tag{8}$$

It is remarkable that for the special case of pair-wise interactions the diagonal elements k_{ii} of the total atomic level stiffness tensor can be represented as a sum over corresponding off-diagonal elements k_{ij}

$$k_{ii} = -E^{\text{int}}_{,r_i r_i} = -\sum_{j \neq i} k_{ij} \tag{9}$$

3. Continuum-atomistic constitutive modelling

Next we pursue a description of the above mentioned mixed continuum-atomistic approach which is e.g. employed among other, more sophisticated concepts by Tadmor (1996) and Ortiz and Phillips (1996) as well as by Shenoy et al. (1999). The key idea here is to replace the phenomenological macroscopic strain energy density W_0 per unit volume in the material configuration by appropriate atomistic potentials. This step allows in a natural way to consider a real crystal structure with the appropriate anisotropic energy density in the setting of continuum mechanics. In the sequel, we will denote this hybrid model the continuum-atomistic model. Thereby the important step is to find a correspondence between an atomistic energy function E_i and a specific strain energy density W_0. By the assumption that the individual atomic contributions to the total energy can be defined and that the energy of each atom i is uniformly distributed over the volume V_i of its Voronoi polyhedron in Fig 5, see Tadmor (1996), both energies can be related as follows

$$W_0 \doteq \frac{E_i(r_{i1}, \ldots, r_{iN})}{V_i} = \frac{1}{2V_i} \sum_{j \neq i} \Phi_{ij} = W_0(r_{i1}, \ldots, r_{iN}) \tag{10}$$

The remaining problem is now to establish a relation between the continuum deformation and the atomic distance vectors. Here we shall follow two approaches in the sequel, namely the first and the newly proposed second-order CBR.

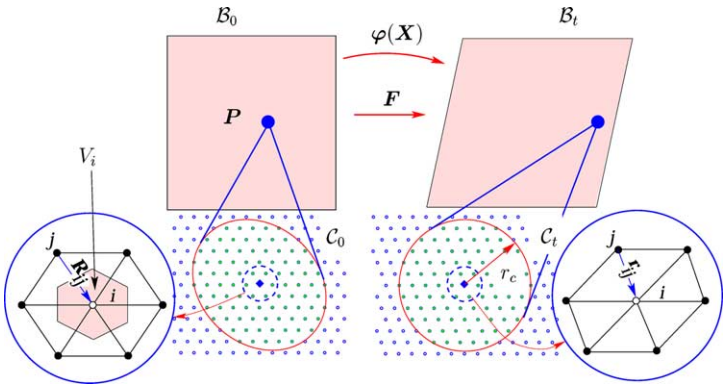

Fig. 5. The first-order Cauchy–Born rule for the case of homogeneous deformation.

3.1. Kinematics of continuum mechanics

In order to facilitate the further discussion we firstly give a short review of the kinematics in the framework of continuum mechanics. In this approach, the non-linear deformation map $\boldsymbol{\varphi}(\boldsymbol{X})$ relates the placement $\boldsymbol{X}$ in the material configuration $\mathscr{B}_0$ to the placement $\boldsymbol{x} = \boldsymbol{\varphi}(\boldsymbol{X})$ in the spatial configuration $\mathscr{B}_t$, see the upper part of Fig. 5. Thereby, the first-order deformation gradient $\boldsymbol{F}$ defines a linear tangent map and is given by the two-point tensor $\boldsymbol{F} \doteq \nabla_{\boldsymbol{X}} \boldsymbol{\varphi}$. In the higher-order theory, the second-order deformation gradient $\boldsymbol{G} \doteq \nabla_{\boldsymbol{X}} \nabla_{\boldsymbol{X}} \boldsymbol{\varphi}$, a rank-three tensor, can be introduced in addition.

3.2. First-order Cauchy–Born rule

The conceptual idea is here to consider homogeneous deformations of an infinite representative crystallite, whereby the kinematic relation is given by the first-order Cauchy–Born rule, see the introduction. Here it is assumed that the lattice vectors $\boldsymbol{r}_{ij}$ of the spatial configuration result from the corresponding $\boldsymbol{R}_{ij}$ in the material configuration by the application of the local deformation gradient $\boldsymbol{F} = \nabla_{\boldsymbol{X}} \boldsymbol{\varphi}$ (which in general varies with $\boldsymbol{X}$), see Fig. 5,

$$\boldsymbol{r}_{ij} = \boldsymbol{F} \cdot \boldsymbol{R}_{ij} \tag{11}$$

Then, the strain energy density W_0 defined in (10) depends only on relative distances r_{ij} between the atom i and all other atoms and can formally be represented as a function of the deformation gradient and the fixed distance vectors $\boldsymbol{R}_{ij}$ in the material configuration

$$W_0 = W_0(r_{i1}, \ldots, r_{iN}) = W_0(|\boldsymbol{F} \cdot \boldsymbol{R}_{i1}|, \ldots, |\boldsymbol{F} \cdot \boldsymbol{R}_{iN}|) = W_0(\boldsymbol{F}) \tag{12}$$

Here the constant distance vectors $\boldsymbol{R}_{ij}$ in the material configuration are given and depend only on the underlying geometrical crystal lattice structure. Thus, each point of the continuum is modelled by an infinite crystal which deforms homogeneously. In practice the cut-off radius r_c of the pair potential limits the extension of that part of the crystal that has to be considered, see again Fig. 5.

3.3. Euler–Lagrange equations for first-order hyperelastic continua

At this place we reiterate the well-known derivation of the equilibrium equations of a first-order hyperelastic continuum as well as the corresponding boundary conditions in the usual way by minimization of the total potential energy:

$$\delta E^{\mathrm{tot}} = \delta \int_{\mathscr{B}_0} W_0(\boldsymbol{F})\,\mathrm{d}V + \delta E^{\mathrm{ext}} = \int_{\mathscr{B}_0} \frac{\partial W_0}{\partial \boldsymbol{F}} : \nabla_{\boldsymbol{X}} \delta\boldsymbol{\varphi}\,\mathrm{d}V + \delta E^{\mathrm{ext}} = 0 \tag{13}$$

with the variation of the potential E^{ext} of the external forces

$$\delta E^{\mathrm{ext}} = -\int_{\mathscr{B}_0} \boldsymbol{b}_0 \cdot \delta\boldsymbol{\varphi}\,\mathrm{d}V - \int_{\partial\mathscr{B}_0} \boldsymbol{t}_0^P \cdot \delta\boldsymbol{\varphi}\,\mathrm{d}A \tag{14}$$

whereby $\boldsymbol{b}_0$ is the body force and $\boldsymbol{t}_0^P$ is the nominal surface traction in the material configuration. Here : denotes a double contraction of rank-two tensors $\boldsymbol{P}$ and $\boldsymbol{F}$, i.e. $P_{iJ}F_{iJ}$. After application of partial integration and making use of the Gauss theorem Eq. (13) yields the familiar local equilibrium equations with the conventional Neumann-type boundary conditions in the well-known format

$$\mathrm{Div}\,\boldsymbol{P} + \boldsymbol{b}_0 = \boldsymbol{0} \quad \text{in } \mathscr{B}_0 \tag{15}$$

$$\boldsymbol{P} \cdot \boldsymbol{N} = \boldsymbol{t}_0^P \quad \text{on } \partial\mathscr{B}_0 \tag{16}$$

with the Piola–Kirchhoff stress tensor defined by

$$\boldsymbol{P} \doteq \frac{\partial W_0}{\partial \boldsymbol{F}} \tag{17}$$

and $\boldsymbol{N}$ the material surface normal to $\partial\mathscr{B}_0$. Here, the operator Div denotes the corresponding divergence operation with respect to the material coordinates $\boldsymbol{X}$.

3.4. First-order continuum-atomistic modelling

The constitutive law given by Eq. (17) results under consideration of (10) and (12) in the following explicit format: [1]

$$\boldsymbol{P} = \frac{1}{2V_i} \sum_{j \neq i} \boldsymbol{f}_{ji} \otimes \boldsymbol{R}_{ij} \tag{18}$$

with the consequent symmetry for the appropriate push-forward, i.e. the spatial Kirchhoff stress:

$$\boldsymbol{P} : \nabla_{\boldsymbol{X}} \delta\boldsymbol{\varphi} = [\boldsymbol{P} \cdot \boldsymbol{F}^t] : \nabla_{\boldsymbol{x}} \delta\boldsymbol{\varphi} = \left[\frac{1}{2V_i} \sum_{j \neq i} \boldsymbol{f}_{ji} \otimes \boldsymbol{r}_{ij} \right] : \nabla_{\boldsymbol{x}} \delta\boldsymbol{\varphi} \tag{19}$$

Likewise the fourth-order tangent operator $\mathbb{L}$ relating the material rate of $\boldsymbol{P}$ with the material rate of $\boldsymbol{F}$ takes the explicit format

$$\mathbb{L} \doteq \frac{\partial^2 W_0}{\partial \boldsymbol{F} \otimes \partial \boldsymbol{F}} = \frac{1}{2V_i} \sum_{j \neq i} \boldsymbol{k}_{ij} \,\overline{\otimes}\, [\boldsymbol{R}_{ij} \otimes \boldsymbol{R}_{ij}] \tag{20}$$

Here $\boldsymbol{f}_{ji} = -\boldsymbol{f}_{ij}$ and $\boldsymbol{k}_{ij}$ are defined as in (6) and (8), respectively. [2] It is remarkable that the quantities which are defined for the underlying atomistic model show up in a simple format in the relations for $\boldsymbol{P}$ and $\mathbb{L}$, thus reflecting the atomistic features in the continuum setting.

[1] A more implicit format of the constitutive law without resorting explicitly to the atomistic interaction forces can be found e.g. in the PhD Thesis of Tadmor (1996).

[2] The non-standard dyadic product $\overline{\otimes}$ emerging in (20) is here introduced for second-order tensors $\boldsymbol{A}$, $\boldsymbol{B}$ and $\boldsymbol{C}$ as $[\boldsymbol{A} \,\overline{\otimes}\, \boldsymbol{B}] : \boldsymbol{C} = \boldsymbol{A} \cdot \boldsymbol{C} \cdot \boldsymbol{B}^t$ or $[\boldsymbol{A} \,\overline{\otimes}\, \boldsymbol{B}]_{ijkl} \doteq A_{ik}B_{jl}$.

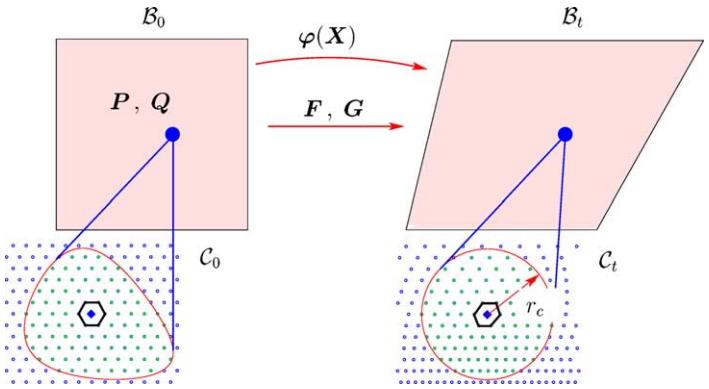

Fig. 6. The second-order Cauchy–Born rule for the case of non-homogeneous deformation.

3.5. Second-order Cauchy–Born rule

The Cauchy–Born rule in the form (11) is insufficient to describe the kinematics for the case of inhomogeneous deformations. Furthermore, size effects cannot be taken into account, see e.g. Geers et al. (2001) or Fleck and Hutchinson (1996), if the problem size reaches the scale of the atomic spacing as in the case of nano mechanics. To get over this discrepancy we take into account the second quadratic term in the Taylor's series expansion of the deformation field. Thereby, (11) is considered as the first term in this expansion. The extended Cauchy–Born rule of second-order can thus be expressed in the following format (Fig. 6)

$$\boldsymbol{r}_{ij} = \boldsymbol{F} \cdot \boldsymbol{R}_{ij} + \tfrac{1}{2}\boldsymbol{G} : [\boldsymbol{R}_{ij} \otimes \boldsymbol{R}_{ij}] \tag{21}$$

with the previously introduced second-order deformation gradient $\boldsymbol{G}$. The strain energy density W_0 now consequently depends on both $\boldsymbol{F}$ and $\boldsymbol{G}$:

$$\begin{aligned} W_0 &= W_0(r_{i1}, \ldots, r_{iN}) = W_0\big(\big|\boldsymbol{F} \cdot \boldsymbol{R}_{i1} + \tfrac{1}{2}\boldsymbol{G} : [\boldsymbol{R}_{i1} \otimes \boldsymbol{R}_{iN}]\big|, \ldots, \big|\boldsymbol{F} \cdot \boldsymbol{R}_{iN} + \tfrac{1}{2}\boldsymbol{G} : [\boldsymbol{R}_{iN} \otimes \boldsymbol{R}_{iN}]\big|\big) \\ &= W_0(\boldsymbol{F}, \boldsymbol{G}) \end{aligned} \tag{22}$$

The Euler–Lagrange equations corresponding to a potential depending on $\boldsymbol{F}$ and $\boldsymbol{G}$ will be presented in the sequel.

3.6. Euler–Lagrange equations for second-order hyperelastic continua

The familiar energy minimization for the second-order hyperelastic continuum takes again a format similar to (13):

$$\begin{aligned} \delta E^{\text{tot}} &= \delta \int_{\mathcal{B}_0} W_0(\boldsymbol{F}, \boldsymbol{G})\, \mathrm{d}V + \delta E^{\text{ext}} \\ &= \int_{\mathcal{B}_0} \left[\frac{\partial W_0}{\partial \boldsymbol{F}} : \nabla_{\boldsymbol{X}} \delta\boldsymbol{\varphi} + \frac{\partial W_0}{\partial \boldsymbol{G}} \vdots \nabla_{\boldsymbol{X}} \nabla_{\boldsymbol{X}} \delta\boldsymbol{\varphi} \right] \mathrm{d}V + \delta E^{\text{ext}} = 0 \end{aligned} \tag{23}$$

Here $\vdots$ denotes a triple contraction of rank-three tensors $\boldsymbol{Q}$ and $\boldsymbol{G}$, i.e. $Q_{iJK}G_{iJK}$. In addition to the Piola–Kirchhoff stress (17), the second-order stress $\boldsymbol{Q}$ is here introduced as the first derivative of the energy density with respect to the second-order deformation gradient $\boldsymbol{G}$:

$$\boldsymbol{Q} \doteq \frac{\partial W_0}{\partial \boldsymbol{G}} \tag{24}$$

It follows from (24) that the second-order stress is represented by a rank-three tensor. The symmetry properties of this tensor are determined by the symmetry of $\boldsymbol{G} = \nabla_{\boldsymbol{X}} \nabla_{\boldsymbol{X}} \delta\boldsymbol{\varphi}$ which is symmetric in the second and third index because of the interchangeability of second partial derivatives. The variation of the external potential includes an additional term due to the second-order stress traction $\boldsymbol{t}_0^Q$ on the surface $\partial\mathscr{B}_0$, see e.g. Mindlin (1965) or Fleck and Hutchinson (1996), and can be represented as a sum of three terms: [3]

$$\delta E^{\text{ext}} = -\int_{\mathscr{B}_0} \delta\boldsymbol{\varphi} \cdot \boldsymbol{b}_0 \, \mathrm{d}V - \int_{\partial\mathscr{B}_0} \delta\boldsymbol{\varphi} \cdot \boldsymbol{t}_0^P \, \mathrm{d}A - \int_{\partial\mathscr{B}_0} \nabla_N \delta\boldsymbol{\varphi} \cdot \boldsymbol{t}_0^Q \, \mathrm{d}A, \tag{25}$$

After simple but tedious transformations of (23) outlined in details in the Appendix A whereby we essentially involve partial integration, the Gauss theorem and the Stoke's surface divergence theorem the following higher-order equilibrium equations and Neumann-type boundary conditions are obtained:

$$\mathrm{Div}(\boldsymbol{P} - \mathrm{Div}\boldsymbol{Q}) + \boldsymbol{b}_0 = \boldsymbol{0} \quad \text{in } \mathscr{B}_0 \tag{26}$$

$$[\boldsymbol{P} - \mathrm{Div}\boldsymbol{Q}] \cdot \boldsymbol{N} + \mathfrak{L}(\boldsymbol{Q} \cdot \boldsymbol{N}) = \boldsymbol{t}_0^P \quad \text{on } \partial\mathscr{B}_0 \tag{27}$$

$$\boldsymbol{Q} : [\boldsymbol{N} \otimes \boldsymbol{N}] = \boldsymbol{t}_0^Q \quad \text{on } \partial\mathscr{B}_0 \tag{28}$$

Thereby $\mathfrak{L}(\boldsymbol{Q} \cdot \boldsymbol{N})$ denotes the following differential operator:

$$-\mathfrak{L}(\boldsymbol{Q} \cdot \boldsymbol{N}) \doteq K\boldsymbol{Q} : [\boldsymbol{N} \otimes \boldsymbol{N}] + \nabla_{\boldsymbol{X}}^{\mathrm{T}}(\boldsymbol{Q} \cdot \boldsymbol{N}) : \boldsymbol{I} \tag{29}$$

with the mean curvature $K \doteq -\nabla_{\boldsymbol{X}}^{\mathrm{T}} \boldsymbol{N} : \boldsymbol{I}$ of the surface $\partial\mathscr{B}_0$, see Brand (1957).

3.7. Second-order continuum-atomistic modelling

The explicit format of the constitutive law for the Piola–Kirchhoff stress retains its form previously given by (18). The definition (24) renders for the second-order stress under consideration of (10) and (22) the following format:

$$\boldsymbol{Q} = \frac{1}{4V_i} \sum_{j \neq i} \boldsymbol{f}_{ji} \otimes \boldsymbol{R}_{ij} \otimes \boldsymbol{R}_{ij} \tag{30}$$

The push-forward operation in the case of the second-order theory is more complicated as in the first-order theory. The specific virtual work transformation yields spatial stress tensors in the following explicit format: [4]

[3] The gradient operator can be decomposed into normal and tangential parts according to the following rule: $\nabla_{\boldsymbol{X}}(\bullet) = [\nabla_{\boldsymbol{X}}(\bullet) \cdot \boldsymbol{N}]\boldsymbol{N} + \nabla_{\boldsymbol{X}}(\bullet) \cdot [\boldsymbol{I} - \boldsymbol{N} \otimes \boldsymbol{N}] \equiv \nabla_{\boldsymbol{X}}^N(\bullet) + \nabla_{\boldsymbol{X}}^{\mathrm{T}}(\bullet)$ with the normal gradient operator $\nabla_{\boldsymbol{X}}^N(\bullet) \doteq [\nabla_{\boldsymbol{X}}(\bullet) \cdot \boldsymbol{N}]\boldsymbol{N} \equiv \nabla_N(\bullet)\boldsymbol{N}$ and the tangential gradient operator $\nabla_{\boldsymbol{X}}^{\mathrm{T}}(\bullet) \doteq \nabla_{\boldsymbol{X}}(\bullet) \cdot [\boldsymbol{I} - \boldsymbol{N} \otimes \boldsymbol{N}]$, whereby $\boldsymbol{N}$ denotes the material surface normal vector.

[4] The opeartion $\overset{2,3}{\vdots}$ denotes the double contraction of two rank-three tensors with respect to their second and third indices, e.g. $[\boldsymbol{Q} \overset{2,3}{\vdots} \boldsymbol{G}]_{ab} \doteq Q_{aMN} G_{bMN}$.

$$\begin{aligned}
&\boldsymbol{P} : \nabla_{\boldsymbol{X}} \delta\boldsymbol{\varphi} + \boldsymbol{Q} \dddot{:} \nabla_{\boldsymbol{X}} \nabla_{\boldsymbol{X}} \delta\boldsymbol{\varphi} \\
&\quad = [\boldsymbol{P} \cdot \boldsymbol{F}^t + \boldsymbol{Q} \overset{2,3}{\dddot{:}} \boldsymbol{G}] : \nabla_{\boldsymbol{x}} \delta\boldsymbol{\varphi} + [\boldsymbol{Q} : [\boldsymbol{F}^t \overline{\otimes} \boldsymbol{F}^t]] \dddot{:} \nabla_{\boldsymbol{x}} \nabla_{\boldsymbol{x}} \delta\boldsymbol{\varphi} \\
&\quad = \left[\frac{1}{2V_i} \sum_{j \neq i} \boldsymbol{f}_{ji} \otimes \boldsymbol{r}_{ij} \right] : \nabla_{\boldsymbol{x}} \delta\boldsymbol{\varphi} + \left[\frac{1}{4V_i} \sum_{j \neq i} \boldsymbol{f}_{ji} \otimes \boldsymbol{r}^1_{ij} \otimes \boldsymbol{r}^1_{ij} \right] \dddot{:} \nabla_{\boldsymbol{x}} \nabla_{\boldsymbol{x}} \delta\boldsymbol{\varphi}
\end{aligned} \tag{31}$$

with the spatial distance vector in the first-order theory $\boldsymbol{r}^1_{ij} \doteq \boldsymbol{R}_{ij} \cdot \boldsymbol{F}^t$. The linearization of (30) yields the sixth-order tangent operator $\mathbb{M}_{GG}$ and the fifth-order tangent operators $\mathbb{M}_{FG}$ and $\mathbb{M}_{GF}$ [5]

$$\mathbb{M}_{FG} \doteq \frac{\partial^2 W_0}{\partial \boldsymbol{F} \otimes \partial \boldsymbol{G}} = \frac{1}{4V_i} \sum_{j \neq i} [\boldsymbol{k}_{ij} \overline{\otimes} [\boldsymbol{R}_{ij} \otimes \boldsymbol{R}_{ij}]] \otimes \boldsymbol{R}_{ij} \tag{32}$$

$$\mathbb{M}_{GF} \doteq \frac{\partial^2 W_0}{\partial \boldsymbol{G} \otimes \partial \boldsymbol{F}} = \frac{1}{4V_i} \sum_{j \neq i} [\boldsymbol{k}_{ij} \underline{\otimes} [\boldsymbol{R}_{ij} \otimes \boldsymbol{R}_{ij}]] \otimes \boldsymbol{R}_{ij} \tag{33}$$

$$\mathbb{M}_{GG} \doteq \frac{\partial^2 W_0}{\partial \boldsymbol{G} \otimes \partial \boldsymbol{G}} = \frac{1}{8V_i} \sum_{j \neq i} [\boldsymbol{k}_{ij} \underline{\otimes} [\boldsymbol{R}_{ij} \otimes \boldsymbol{R}_{ij}]] \otimes [\boldsymbol{R}_{ij} \otimes \boldsymbol{R}_{ij}] \tag{34}$$

The linearization of the Piola–Kirchhoff stress takes again the known format (20).

4. Example

To investigate the influence of the higher-order deformation gradient contribution in the extended Cauchy–Born rule on the accuracy of the kinematic description a special non-homogeneous simple-shear-like deformation has been chosen and studied.

4.1. Geometric characterization of a prototype deformation

Firstly we give a short description of the deformation analysed in the sequel.

4.1.1. Homogeneous simple shear deformation

Before introducing the above mentioned non-homogeneous deformation we briefly recall the main features of the familiar homogeneous simple shear deformation, see Fig. 7. The origin of the local coordinate system is chosen in the middle of the undeformed volume element. All straight vertical lines in the material configuration transform to straight but inclined lines with the same slope α in the spatial configuration. In this case the deformation field $\boldsymbol{\varphi}$ can be represented as a linear map of the material position vectors $\boldsymbol{X}$ as

$$[\boldsymbol{\varphi}] = \begin{bmatrix} \varphi_1 \\ \varphi_2 \end{bmatrix} = \begin{bmatrix} X_1 + BX_2 \\ X_2 \end{bmatrix} \rightsquigarrow \boldsymbol{\varphi} = \boldsymbol{F}^{\mathrm{hom}} \cdot \boldsymbol{X} \tag{35}$$

with the constant deformation gradient in the terms of the shear number γ

[5] The non-standard dyadic product $\underline{\otimes}$ emerging in (33) and (34) is here introduced for second-order tensors $\boldsymbol{A}$, $\boldsymbol{B}$ and $\boldsymbol{C}$ as $[\boldsymbol{A} \underline{\otimes} \boldsymbol{B}] : \boldsymbol{C} = \boldsymbol{A} \cdot \boldsymbol{C}^t \cdot \boldsymbol{B}^t$ or $[\boldsymbol{A} \underline{\otimes} \boldsymbol{B}]_{ijkl} \doteq A_{il} B_{jk}$.

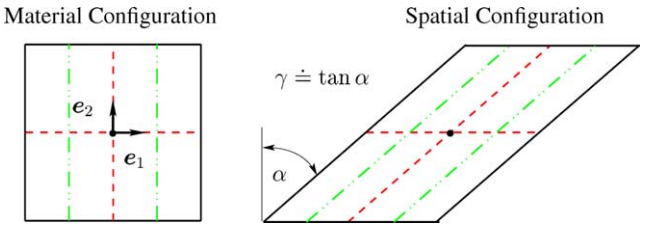

Fig. 7. The homogeneous simple shear deformation with the spatially constant shear number γ.

$$F_{iJ} = F_{iJ}^{\mathrm{hom}}(B) = \frac{\partial \varphi_i}{\partial X_J} = \begin{bmatrix} 1 & \gamma \\ 0 & 1 \end{bmatrix} \quad \text{with} \quad \gamma \equiv B = \text{constant over } \mathscr{B}_0 \tag{36}$$

Clearly, the second-order deformation gradient $\boldsymbol{G}$ vanishes identically in this homogeneous case:

$$G_{iJ1} \equiv \frac{\partial F_{iJ}}{\partial X_1} = \begin{bmatrix} 0 & 0 \\ 0 & 0 \end{bmatrix}, \quad G_{iJ2} \equiv \frac{\partial F_{iJ}}{\partial X_2} = \begin{bmatrix} 0 & 0 \\ 0 & 0 \end{bmatrix} \tag{37}$$

4.1.2. Non-homogeneous simple-shear-like deformation

To get a slightly perturbed simple shear deformation we add a quadratic term with a small parameter $A \ll B$ to the deformation field (35):

$$[\boldsymbol{\varphi}] = \begin{bmatrix} \varphi_1 \\ \varphi_2 \end{bmatrix} = \begin{bmatrix} X_1 + BX_2 + AX_1X_2 \\ X_2 \end{bmatrix} \rightsquigarrow \boldsymbol{\varphi} = \boldsymbol{F}^{\mathrm{hom}} \cdot \boldsymbol{X} + \frac{1}{2}\boldsymbol{G} : [\boldsymbol{X} \otimes \boldsymbol{X}] \tag{38}$$

Note that this deformation is captured by the extended Cauchy–Born rule (21) exactly. The deformation gradient of the perturbed simple shear deformation

$$F_{iJ} = \frac{\partial \varphi_i}{\partial X_J} = \begin{bmatrix} 1 + AX_2 & B + AX_1 \\ 0 & 1 \end{bmatrix} \tag{39}$$

consists of the deformation gradient $\boldsymbol{F}^{\mathrm{hom}}$ of the homogeneous deformation and the perturbation with the small parameter A:

$$F_{iJ} = F_{iJ}^{\mathrm{hom}}(B) + A \begin{bmatrix} X_2 & X_1 \\ 0 & 0 \end{bmatrix} \tag{40}$$

Here, the second-order deformation gradient is a constant for the present case of the quadratic deformation field:

$$G_{iJ1} \equiv \frac{\partial F_{iJ}}{\partial X_1} = \begin{bmatrix} 0 & A \\ 0 & 0 \end{bmatrix}, \quad G_{iJ2} \equiv \frac{\partial F_{iJ}}{\partial X_2} = \begin{bmatrix} A & 0 \\ 0 & 0 \end{bmatrix} \tag{41}$$

Interesting enough the deformation (38) can be represented in a format which appears similar to the common simple shear deformation

$$\boldsymbol{\varphi} = \boldsymbol{F}^{\mathrm{inhom}} \cdot \boldsymbol{X}, \quad F_{iJ}^{\mathrm{inhom}} = \begin{bmatrix} 1 & \gamma(\boldsymbol{X}) \\ 0 & 1 \end{bmatrix} \neq F_{iJ} \tag{42}$$

Note however that the non-linear map $\boldsymbol{F}^{\mathrm{inhom}}$ differs from the deformation gradient $\boldsymbol{F}$. The shear number γ is no more constant over $\mathscr{B}_0$ and depends on the component X_1 of the material position vector $\boldsymbol{X}$:

$$\gamma(\boldsymbol{X}) = B + AX_1 \tag{43}$$

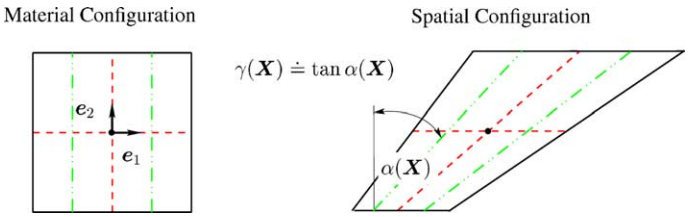

Fig. 8. The non-homogeneous simple-shear-like deformation with the position-depending shear number $\gamma(\boldsymbol{X})$.

Thus straight vertical lines in the material configuration transform to straight lines in the spatial configuration with a slope depending on the material coordinate X_1, see Fig. 8.

4.2. Detailed investigations

To investigate the influence of the higher-order gradient the chosen non-homogeneous deformation has been studied for various ratios A/B. To describe the interatomic interaction the above mentioned Lennard-Jones pair potential (2) with material parameters fitted to aluminium, i.e. $\sigma = 0.2575$ nm and $\varepsilon = 0.1699$ nN nm, is used as a prototype model. These parameters are obtained by a fitting procedure under the constraint of a stress free material configuration and equality of the atomic energy in the material configuration to the sublimation energy of aluminium, i.e. $E^{\text{sub}} = 3.58$ eV $= 0.574$ nN nm. Thereby the cut-off radius r_c is chosen to equal five atomic spacings, i.e. $r_0 = 0.286$ nm.

Fig. 9 depicts the material and spatial collection of atoms representing the crystal of interest for two ratios A/B, whereby $A/B = 0$ corresponds to the homogeneous deformation field (35). The circles in the spatial configuration contain the next neighbours of the atoms in their centers where the deformation field has its origin. The deformed ellipses correspond to these circles pulled back by the deformation to the material configuration. [6] It is easy to recognize that the consideration of the second-order deformation leads to a change of the spatial configuration even for the small ratio $A/B = 0.1$. This could better be observed in Fig. 10 where the next neighbours distributions for three different ratios $A/B > 0$ are compared with such distribution for $A/B = 0$ corresponding to the homogeneous deformation. On the right-hand side, the regions in which the circles and triangles overlap denote regions of a homogeneous deformation state. The homogeneous and non-homogeneous deformation fields lead roughly to the same displacement in these regions. With increasing A/B these regions tend to become smaller. Fig. 11 represents this observation even better. Here each figure, except from the first one, is an overlay of two spatial configurations. One of them is deformed homogeneously ($A/B = 0$) and the other one non-homogeneously with corresponding ratio A/B varying from 0.01 to 0.25. It is plausible that the decision whether the deformation is homogeneous enough such that the standard Cauchy–Born rule applies or if it should be treated as a non-homogeneous deformation depends on the length of the cut-off radius r_c. For instance, the deformation in the case $A/B = 0.02$ cannot be considered as homogeneous if $r_c \gtrsim 2r_0$, whereby r_0 denotes the lattice constant, i.e the atomic spacing.

The energy of the central atom for various ratios A/B has been chosen as further qualitative criterion of inhomogeneity. Thereby, B increases from 0 to 3.48 continuously. Fig. 12 shows the corresponding energy curves together with the snap-shots of the atom distribution within the cut-off circle for special values of B.

[6] To obtain a deformed ellipse depicting the boundary of the next neighbours of the atom i in the material configuration the circle in the spatial configuration must be pulled back to the material configuration. In general this is connected with the solution of the non-linear system of algebraic equations (38) with respect to X_1 and X_2. In the special case chosen here $X_2 = \varphi_2$ remains constant and this renders X_1 simply by substituting X_2 in the first row of (38).

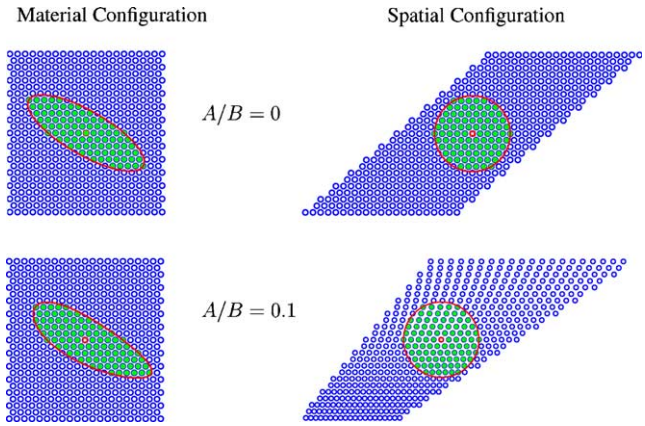

Fig. 9. The material (on the left-hand side) and spatial configuration according to (38). Prototype model configuration for $A/B = 0$ (homogeneous deformation) and $A/B = 0.1$ (inhomogeneous deformation). The right-hand side corresponds to $B = 1.16$.

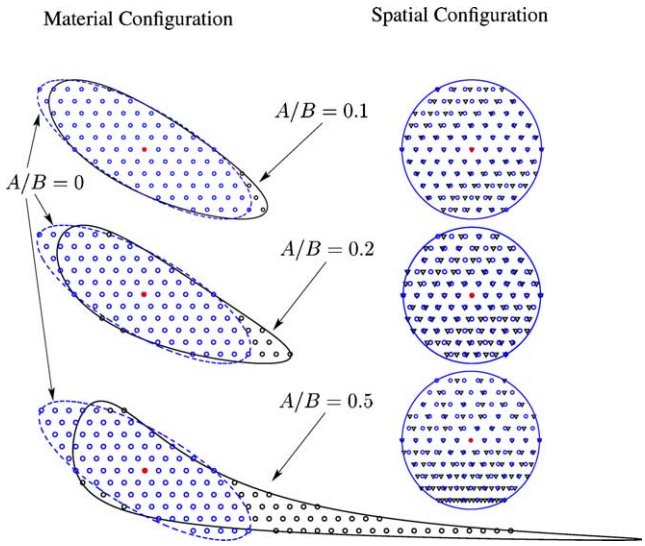

Fig. 10. The next neighbours of the central atom in the material and spatial configurations for different ratios A/B (solid lines on the left-hand side) pared with the next neighbours distribution in the case of the homogeneous deformation $A/B = 0$ (dashed line on the left-hand side). The atoms in the case of the non-homogeneous deformation are represented as triangles on the right-hand side. The circles correspond to a homogeneous deformation. Both cases coincide in the material configuration. The right-hand side corresponds to $B = 1.16$.

The first curve is strongly periodic since the reference crystal structure repeats itself periodically during the homogeneous simple shear deformation. Particularly, for the chosen structure the energy becomes minimal for the shear numbers $B = 1.16$, 2.32 and so on. All the snap-shots correspond to the repeating reference crystal structure and the three first minima of the energy curve for homogeneous deformation. The energy curves differ more and more from this curve with increasing ratio A/B. Nevertheless it can be observed that the energy change for the given parameter set is non-essential within the first period. This can be attributed

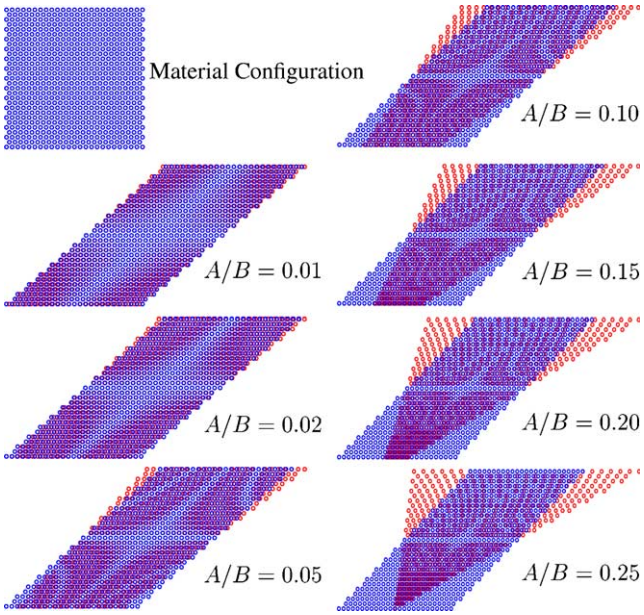

Fig. 11. The overlay of two spatial configurations of a homogeneously and a non-homogeneously deformed material area with various ratios A/B. The deformed state corresponds to $B = 1.16$.

especially to the short range interaction of the pair potential we used. In conclusion a simple quantitative inhomogeneity criterion should be elaborated.

4.3. Simple deformation inhomogeneity measure

The essential information about the deformation field inhomogeneity is contained in the second-order deformation gradient $\boldsymbol{G}$ which is anyway needed within the gradient extended framework. For the planar case $\boldsymbol{G}$ consists of the four vectors:

$$[\boldsymbol{G}] \doteq \left[\frac{\partial \boldsymbol{F}}{\partial \boldsymbol{X}}\right] = \begin{bmatrix} \dfrac{\partial F_{11}}{\partial \boldsymbol{X}} & \dfrac{\partial F_{12}}{\partial \boldsymbol{X}} \\ \dfrac{\partial F_{21}}{\partial \boldsymbol{X}} & \dfrac{\partial F_{22}}{\partial \boldsymbol{X}} \end{bmatrix} \tag{44}$$

Next, we compose the matrix $\boldsymbol{D}(\boldsymbol{X})$ from components which are the norms of the corresponding components of $\boldsymbol{G}$:

$$[\boldsymbol{D}(\boldsymbol{X})] \doteq \begin{bmatrix} \left\| \dfrac{\partial F_{11}}{\partial \boldsymbol{X}} \right\| & \left\| \dfrac{\partial F_{12}}{\partial \boldsymbol{X}} \right\| \\ \left\| \dfrac{\partial F_{21}}{\partial \boldsymbol{X}} \right\| & \left\| \dfrac{\partial F_{22}}{\partial \boldsymbol{X}} \right\| \end{bmatrix} \equiv \begin{bmatrix} D_{11}(\boldsymbol{X}) & D_{12}(\boldsymbol{X}) \\ D_{21}(\boldsymbol{X}) & D_{22}(\boldsymbol{X}) \end{bmatrix} \tag{45}$$

Each component must be evaluated at the site of each atom from the next neighbours list in the cut-off circle and the maximum value must be found:

$$D^{\max} \doteq \max_{i,J} \left\{ \max_{\boldsymbol{X}} \{D_{iJ}(\boldsymbol{X})\} \right\} \tag{46}$$

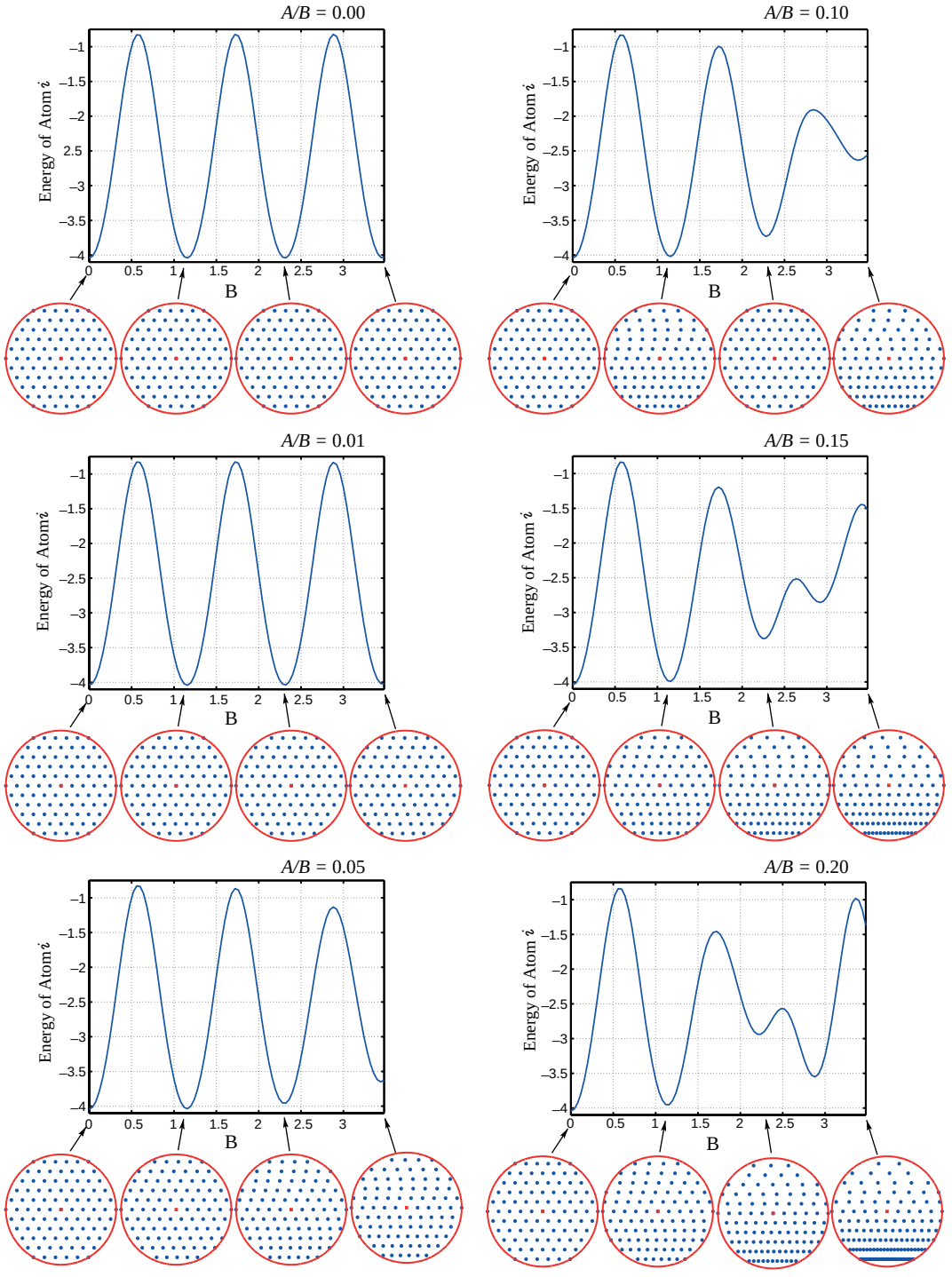

Fig. 12. The energy of the atom in the center of the cut-off circle for various ratios A/B, whereby B increases from 0 to 3.48 continuously. The snap-shots of the atomic distribution within the cut-off circle correspond to the minima of the energy curve for the case of homogeneous deformation $(A/B = 0)$.

$D^{\max}$ has dimension of an inverse length and we thus introduce the inhomogeneity length as the inverse value of $D^{\max}$:

$$L \doteq \frac{1}{D^{\max}} \tag{47}$$

Now we define the deformation inhomogeneity measure as the ratio of the cut-off radius and the inhomogeneity length:

$$\varepsilon \doteq \frac{r_c}{L} = \max_{i,J} \left\{ \max_{X} \{D_{iJ}(\boldsymbol{X})\} \right\} r_c \tag{48}$$

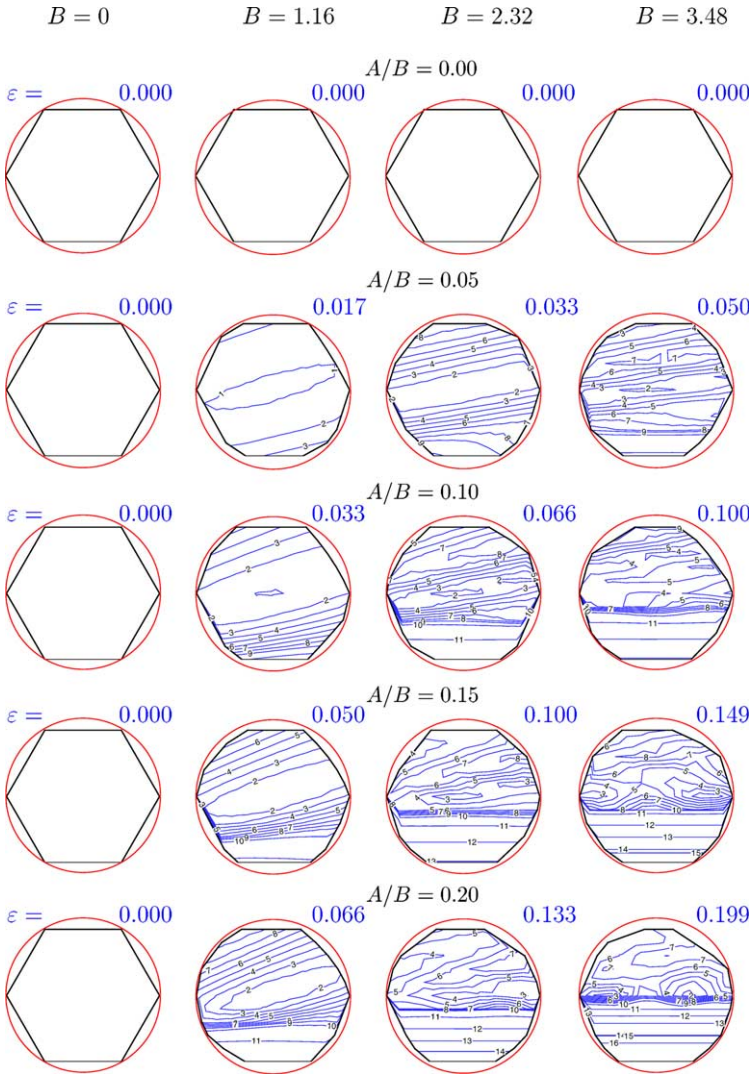

Fig. 13. The energy distribution within the cut-off circle for various ratios A/B and B increasing from 0 to 3.48. The corresponding values of ε computed according to (50) are given additionally. The correspondence between the energy levels numbering and the energy values is given in Table 1.

Table 1
The enumeration of the energy levels as shown in Fig. 13

Number	1	2	3	4	5	6	7	8	9	10	11	12	13	14	15	16
Value [$\times 10^{-18}$ J]	−4.0	−3.5	−3.0	−2.5	−2.0	−1.5	−1.0	−0.5	0.0	1	10	10^2	10^3	10^4	10^5	10^6

This measure characterizes how rapidly the deformation field changes within the cut-off circle. For a homogeneous deformation L tends to infinite and thus ε tends to zero. The question which ε should be chosen as a critical value indicating that a sufficiently non-homogeneous deformation occurs depends on the problem and needs a further study.

In the example considered in the above the first and the second deformation gradients are given by (39) and (41). Then the matrix $\boldsymbol{D}$ is constant and can be represented as follows:

$$[\boldsymbol{D}(\boldsymbol{X})] = \begin{bmatrix} \sqrt{[0^2 + A^2]} & \sqrt{[A^2 + 0^2]} \\ 0 & 0 \end{bmatrix} = \begin{bmatrix} A & A \\ 0 & 0 \end{bmatrix} \tag{49}$$

Consequently, we obtain for L and ε under consideration of (47)–(49):

$$L = \frac{1}{A} \quad \varepsilon = A\, r_c \tag{50}$$

To determine the correspondence between the introduced measure ε and the inhomogeneity we compute the energy level curves shown in Fig. 12 for each atom within the cut-off circle for various A/B and represent this data in the form of energy isolines as shown in Fig. 13. The isolines are numbered according to Table 1. The minimal energy level corresponds to the energy of an atom in the reference lattice. The first nine levels are equidistant with the interval 0.5. Because of the format of the used pair potential given in the 3 the energy under compression tends to enormous positive values due to the reduction of the distances between the atoms in such areas. Thus the levels 10–16 correspond to such positive energy values. In Fig. 13, the areas occupied by the next neighbours of the center atom are shown within the cut-off circle together with the energy distribution in these areas. The corresponding ε computed according to (50) are depicted additionally. As expected, ε vanishes for the homogeneously distributed energy (first column and first row). With increasing A/B and B the energy distribution becomes more and more inhomogeneous and ε increases simultaneously. Apparently, as already mentioned above, the theory-based critical value of ε corresponding to a still sufficiently homogeneous deformation field depends on the problem and the cut-off radius. In our particular case only the energy distribution in the second column and in the first two upper figures of the third column can be considered as homogeneous enough in the vicinity of the center atom. In this case $\varepsilon^{\max} \approx 0.066$.

5. Conclusion

In this work, the extended continuum-atomistic framework based on the second-order Cauchy–Born rule has been introduced for the first time and the corresponding equilibrium equations with appropriate boundary conditions as well as the linearization needed within the iterative solution strategy have been presented for the case of finite deformations, see (30)–(32). Furthermore, on the basis of the simple example of a non-homogeneous deformation field we have demonstrated the influence and importance of the second-order deformation gradient for the computation of the correct spatial configuration in terms of the extended Cauchy–Born assumption. For the sake of the transparency all derivations and results are presented compactly in the tensor format.

It is shown that the newly introduced deformation inhomogeneity measure ε characterizes indirectly the change of deformation field within the interaction circle. The applicability and universality as well as the physical meaning of this measure deserve a further detailed study.

The presented work contains mainly qualitative considerations about the relevance of the higher-order deformation gradient. As an additional motivation (besides capturing of inhomogeneous deformation at the atomic scale) we propose the application of the higher-order gradient formulation in order to guarantee the lower size bound for microstructures that arise due to the loss of infinitesimal rank-one convexity. The aim of our further studies is to discretize and to implement the equilibrium conditions and to solve boundary value problems (BVP) based on the gradient-extended theory similar to the case of small deformations investigated by Shu et al. (1999).

Besides the BVP we furthermore intend to elaborate a failure condition based on the gradient-extended formulation similar to our recent investigation on the basis of the first-order theory, see Sunyk and Steinmann (2001a,b).

Appendix A. Derivation of the higher-order equilibrium and boundary conditions

Here we give the main steps of the derivation of the higher-order equilibrium and boundary conditions (26)–(28). Firstly, Eq. (23) is partially integrated (the second term two times):

$$\begin{aligned}
\delta E^{\text{int}} &= \int_{\mathscr{B}_0} \boldsymbol{P} : \delta\boldsymbol{F} + \boldsymbol{Q} \vdots \delta\boldsymbol{G}\,\mathrm{d}V \\
&= \int_{\mathscr{B}_0} \mathrm{Div}(\delta\boldsymbol{\varphi}\cdot\boldsymbol{P})\,\mathrm{d}V - \int_{\mathscr{B}_0} \delta\boldsymbol{\varphi}\cdot\mathrm{Div}\boldsymbol{P}\,\mathrm{d}V \\
&\quad + \int_{\mathscr{B}_0} \mathrm{Div}(\delta\boldsymbol{F} : \boldsymbol{Q})\,\mathrm{d}V - \int_{\mathscr{B}_0} \delta\boldsymbol{F} : \mathrm{Div}\boldsymbol{Q}\,\mathrm{d}V \\
&= \int_{\mathscr{B}_0} \mathrm{Div}(\delta\boldsymbol{\varphi}\cdot\boldsymbol{P})\,\mathrm{d}V - \int_{\mathscr{B}_0} \delta\boldsymbol{\varphi}\cdot\mathrm{Div}\boldsymbol{P}\,\mathrm{d}V \\
&\quad + \int_{\mathscr{B}_0} \mathrm{Div}(\delta\boldsymbol{F} : \boldsymbol{Q})\,\mathrm{d}V - \int_{\mathscr{B}_0} \mathrm{Div}(\delta\boldsymbol{\varphi}\cdot\mathrm{Div}\boldsymbol{Q})\,\mathrm{d}V + \int_{\mathscr{B}_0} \delta\boldsymbol{\varphi}\cdot\mathrm{Div}(\mathrm{Div}\boldsymbol{Q})\,\mathrm{d}V
\end{aligned} \tag{A.1}$$

After application of the Gauss theorem on the first, third and fourth terms of the last expression and grouping of corresponding terms we obtain:

$$\delta E^{\text{int}} = \int_{\mathscr{B}_0} \delta\boldsymbol{\varphi}\cdot\mathrm{Div}[\mathrm{Div}\boldsymbol{Q} - \boldsymbol{P}]\,\mathrm{d}V + \int_{\partial\mathscr{B}_0} \delta\boldsymbol{\varphi}\cdot[\boldsymbol{P} - \mathrm{Div}\boldsymbol{Q}]\cdot\boldsymbol{N}\,\mathrm{d}A + \int_{\partial\mathscr{B}_0} \delta\boldsymbol{F} : [\boldsymbol{Q}\cdot\boldsymbol{N}]\,\mathrm{d}A \tag{A.2}$$

The first and second terms of (A.2) contribute to (26) and (27) respectively. The variation of $\boldsymbol{F} = \nabla_{\boldsymbol{X}}\boldsymbol{\varphi}$ in the third term is not independent of the variation of $\boldsymbol{\varphi}$ on $\partial\mathscr{B}_0$ because if $\delta\boldsymbol{\varphi}$ is known on $\partial\mathscr{B}_0$, so is the surface gradient of $\delta\boldsymbol{\varphi}$, see Mindlin (1965). Therefore this term cannot directly contribute to the boundary conditions and should be further transformed.

Here, the above mentioned material gradient decomposition into normal and tangential parts is used and we obtain:

$$\int_{\partial\mathscr{B}_0} \nabla_{\boldsymbol{X}}\delta\boldsymbol{\varphi} : [\boldsymbol{Q}\cdot\boldsymbol{N}]\,\mathrm{d}A = \int_{\partial\mathscr{B}_0} \nabla_N\delta\boldsymbol{\varphi}\cdot[\boldsymbol{Q} : [\boldsymbol{N}\otimes\boldsymbol{N}]]\,\mathrm{d}A + \int_{\partial\mathscr{B}_0} \nabla_{\boldsymbol{X}}^{\mathrm{T}}\delta\boldsymbol{\varphi} : [\boldsymbol{Q}\cdot\boldsymbol{N}]\,\mathrm{d}A \tag{A.3}$$

The first term contains independent variations $\nabla_N\,\delta\boldsymbol{\varphi}$ and results in (28). The second term should be partially integrated:

$$\int_{\partial\mathscr{B}_0} \nabla_{\boldsymbol{X}}^{\mathrm{T}}\delta\boldsymbol{\varphi} : [\boldsymbol{Q}\cdot\boldsymbol{N}]\,\mathrm{d}A \equiv \int_{\partial\mathscr{B}_0} [\nabla_{\boldsymbol{X}}\delta\boldsymbol{\varphi}\cdot\boldsymbol{T}] : [\boldsymbol{Q}\cdot\boldsymbol{N}]\,\mathrm{d}A = \int_{\partial\mathscr{B}_0} \nabla_{\boldsymbol{X}}(\delta\boldsymbol{\varphi}\cdot[\boldsymbol{Q}\cdot\boldsymbol{N}]) : \boldsymbol{T}\,\mathrm{d}A - \int_{\partial\mathscr{B}_0} \delta\boldsymbol{\varphi}\cdot\nabla_{\boldsymbol{X}}(\boldsymbol{Q}\cdot\boldsymbol{N}) : \boldsymbol{T}\,\mathrm{d}A \tag{A.4}$$

with $\boldsymbol{T} \doteq [\boldsymbol{I} - \boldsymbol{N}\otimes\boldsymbol{N}]$. Now, the first term of the last expression of (A.4) can be transformed according to the so-called surface divergence theorem stemming essentially from the well-known Stokes theorem for the closed surface $\partial\mathscr{B}_0$, see Brand (1957):

$$\int_{\partial\mathscr{B}_0} (\nabla_{\boldsymbol{X}}\boldsymbol{v} : \boldsymbol{T} + K\boldsymbol{v}\cdot\boldsymbol{N})\,\mathrm{d}A = 0 \tag{A.5}$$

whereby $K \doteq -\nabla_{\boldsymbol{X}}\boldsymbol{N} : \boldsymbol{T} = -\nabla_{\boldsymbol{X}}^{\mathrm{T}}\boldsymbol{N} : \boldsymbol{I}$ is the mean curvature of the surface $\partial\mathscr{B}_0$ and $\boldsymbol{v}$ is a vector. Application of this transformation leads to the final format of the second integral in (A.3):

$$\begin{aligned}
&\int_{\partial\mathscr{B}_0} \nabla_{\boldsymbol{X}}^{\mathrm{T}}\delta\boldsymbol{\varphi} : [\boldsymbol{Q}\cdot\boldsymbol{N}]\,\mathrm{d}A \\
&\quad = -\int_{\partial\mathscr{B}_0} K[\delta\boldsymbol{\varphi}\cdot[\boldsymbol{Q}\cdot\boldsymbol{N}]]\cdot\boldsymbol{N}\,\mathrm{d}A - \int_{\partial\mathscr{B}_0} \delta\boldsymbol{\varphi}\cdot\nabla_{\boldsymbol{X}}(\boldsymbol{Q}\cdot\boldsymbol{N}) : \boldsymbol{T}\,\mathrm{d}A \\
&\quad = -\int_{\partial\mathscr{B}_0} \delta\boldsymbol{\varphi}\cdot[K\boldsymbol{Q} : [\boldsymbol{N}\otimes\boldsymbol{N}] + \nabla_{\boldsymbol{X}}^{\mathrm{T}}(\boldsymbol{Q}\cdot\boldsymbol{N}) : \boldsymbol{I}]\,\mathrm{d}A \\
&\quad \equiv \int_{\partial\mathscr{B}_0} \delta\boldsymbol{\varphi}\cdot\mathfrak{Q}(\boldsymbol{Q}\cdot\boldsymbol{N})\,\mathrm{d}A
\end{aligned} \tag{A.6}$$

Here, the differential operator $\mathfrak{Q}$ is defined as

$$\mathfrak{Q}(\bullet) \doteq -K(\bullet)\cdot\boldsymbol{N} - \nabla_{\boldsymbol{X}}^{\mathrm{T}}(\bullet) : \boldsymbol{I} \tag{A.7}$$

With the Ansatz (A.6) and under consideration of (A.3) the variation of the total energy (A.2) results in

$$\begin{aligned}
\delta E^{\mathrm{tot}} = &\int_{\mathscr{B}_0} \delta\boldsymbol{\varphi}\cdot\mathrm{Div}[\mathrm{Div}\boldsymbol{Q} - \boldsymbol{P}]\,\mathrm{d}V \\
&+ \int_{\partial\mathscr{B}_0} \delta\boldsymbol{\varphi}\cdot[[\boldsymbol{P} - \mathrm{Div}\boldsymbol{Q}]\cdot\boldsymbol{N} + \mathfrak{Q}(\boldsymbol{Q}\cdot\boldsymbol{N})]\,\mathrm{d}A \\
&+ \int_{\partial\mathscr{B}_0} \nabla_N\delta\boldsymbol{\varphi}\cdot[\boldsymbol{Q} : [\boldsymbol{N}\otimes\boldsymbol{N}]]\,\mathrm{d}A + \delta E^{\mathrm{ext}} = 0
\end{aligned} \tag{A.8}$$

Each integrand in this expression contains only independent variations and therefore the equilibrium and boundary conditions can be written in the format (26)–(28).

References

Allen, M.P., Tildesley, D.J., 1987. Computer Simulation of Liquids. Oxford University Press.

Arroyo, M., Belytschko, T., 2002. An atomistic-based finite deformation membrane for single crystalline films. J. Mech. Phys. Solids 50, 1941–1977.

Baskes, M.I., Daw, M.S., 1983. Semiempirical, quantum mechanical calculation of hydrogen embrittlement in metals. Phys. Rev. Lett. 50, 1285.

Born, M., Huang, K., 1954. Dynamical Theory of Crystal Lattices. Clarendon Press, Oxford.

Brand, L., 1957. Vector and Tensor Analysis. Wiley, New York.

Chipot, M., Kinderlehrer, D., 1988. Equilibrium configurations in crystals. Arch. Ration. Mech. Anal. 103, 237–277.

Ericksen, J.L., 1984. Phase Transformations and Material Instabilities in Solids. Academic Press.

Fleck, N.A., Hutchinson, J.W., 1996. Strain gradient plasticity. Adv. Appl. Mech., 33.
Friesecke, G., Theil, F., 2002. Convexity conditions and existence theorems in nonlinear elasticity. J. Nonlinear Sci. 12, 445–478.
Geers, M.G.D., Kouznetsova, V., Brekelmans, W.A.M., 2001. Gradient-enhanced computational homogenization for the micro-macro scale transition. J. Phys. IV 11, 145–152.
Kouznetsova, V., Geers, M.G.D., Brekelmans, W.A.M., 2002. Multi-scale constitutive modelling of heterogeneous materials with a gradient-enhanced computational homogenization scheme. Int. J. Numer. Meth. Eng. 54 (8), 1235–1260.
Milstein, F., 1982. Mechanics of Solids. Pergamon Press, Oxford.
Mindlin, R.D., 1964. Micro-structure in linear elasticity. Arch. Ration. Mech. Anal. 16, 51–78.
Mindlin, R.D., 1965. Second gradient in strain and surface tension in linear elasticity. Int. J. Solids Struct. 1, 417–438.
Nakane, M., Shizava, K., Takahashi, K., 2000. Macroscopic discussions of macroscopic balance equations for solids based on atomistic configurations. Arch. Appl. Mech. 70, 533–549.
Ortiz, M., Phillips, R., 1996. Quasicontinuum analysis of defects in solids. Philos. Mag. A 73, 1529–1563.
Ortiz, M., Phillips, R., 1999. Nanomechanics of defects in solids. Adv. Appl. Mech. 36, 1–71.
Phillips, R., 2001. Crystals, Defects and Microstructures. Cambridge University Press.
Puska, M.J., Nieminen, R.M., Manninen, M., 1981. Atoms embedded in an electron gas: Immersion energies. Phys. Rev. B 24, 3037.
Shenoy, V.B., Miller, R., Tadmor, E.B., Rodney, D., Phillips, R., Ortiz, M., 1999. An adaptive finite element approach to atomic-scale mechanics—the quasicontinuum method. J. Mech. Phys. Solids 47, 611–642.
Shu, J.Y., King, W.E., Fleck, N.A., 1999. Finite elements for materials with strain gradient effects. Int. J. Numer. Methods Eng. 44, 373–391.
Sunyk, R., Steinmann, P., 2001a. Localization analysis of mixed continuum-atomistic models. J. Phys. IV 11, 251–258.
Sunyk, R., Steinmann, P., 2001b. Mixed continuum-atomistic analysis of single crystals. In: Diebels, S. (Ed.), Zur Beschreibung komplexen Materialverhaltens. University of Stuttgart, pp. 175–188.
Tadmor, E.B., 1996. The quasicontinuum method. Ph.D. Thesis, Brown University.
Tadmor, E.B., Smith, G.S., Bernstein, N., Kaxiras, E., 1999. Mixed finite element and atomistic formulation for complex crystals. Phys. Rev. B 59, 235–245.
Toupin, R.A., 1962. Elastic materials with couple stresses. Arch. Ration. Mech. Anal. 11, 385–414.
Zanzotto, G., 1996. The Cauchy–Born hypothesis, nonlinear elasticity and mechanical twinning in crystals. Acta Cryst. A 52, 839–849.